ELSEVIER

Journal of Nuclear Materials 276 (2000) 154–165

journal of nuclear materials

www.elsevier.nl/locate/jnucmat

3D dislocation dynamics: stress–strain behavior and hardening mechanisms in fcc and bcc metals

Hussein M. Zbib[a,*], Tomas Díaz de la Rubia[b], Moono Rhee[b], John P. Hirth[a]

[a] *School of Mechanical and Materials Engineering, Washington State University, Pullman, WA 99164-2920, USA*
[b] *Lawrence Livermore National Laboratory, Livermore, CA 94550, USA*

Abstract

A dislocation dynamics (DD) model for plastic deformation, connecting the macroscopic mechanical properties to basic physical laws governing dislocation mobility and related interaction mechanisms, has been developed. In this model there is a set of critical reactions that determine the overall results of the simulations, such as the stress–strain curve. These reactions are annihilation, formation of jogs, junctions, and dipoles and cross-slip. In this paper, we discuss these reactions and the manner in which they influence the simulated stress–strain behavior of fcc and bcc metals. In particular, we examine the formation (zipping) and strength of dipoles and junctions, and effect of jogs, using the dislocation dynamics model. We show that the strengths (unzipping) of these reactions for various configurations can be determined by direct evaluation of the elastic interactions. Next, we investigate the phenomenon of hardening in metals subjected to cascade damage. The investigated microstructure consists of small dislocation loops decorating the mobile dislocations. Preliminary results reveal that these loops act as hardening agents, trapping the dislocations and resulting in increased yield stress.

1. Introduction

Constitutive modeling of deformation of metals under various loading conditions depends critically on our understanding of the relationship between the macroscopic mechanical properties and the underlying defect sub-structures (e.g. point defect, dislocations, planar defects, precipitates, etc.). Such structures can be highly heterogeneous and in the case of linear defects include dislocation cells, slip bands, microshear bands, persistent slip bands and dislocation tangles, all of which are critical to material properties [1–7]. Understanding how these structures form and evolve and how they affect work hardening is, perhaps, one of the most difficult tasks which is still rife with controversy. The main difficulty has been in dealing with large numbers of dislocations. For example, Kuhlmann-Wilsdorf [7] has proposed that the structures can be understood as a progression of low energy thermodynamic states with something like a conventional phase transition taking place between carpet structures and 3D cell structures at the end of Stage II. However, Holt [8] proposed that dislocation structure evolution can be viewed in the spirit of spinodal decomposition by the introduction of local densities of diffusing dislocation populations. This approach has been adopted in later models. In particular, Walgraef and Aifantis [9] developed a model of dislocation patterning to describe the evolution of ordered structures in chemically reacting systems. In this model, several types of dislocation populations are introduced as density functions of position in space, with the evolution determined by diffusion and reaction terms. Although these reaction–diffusion schemes have been successful in modeling 2D dislocation patterns, they present a number of difficulties associated with determination of model parameters and they do not yet address realistic 3D dislocation configurations.

By viewing the dislocation structures problem as a dynamical system, one can develop a number of discrete models to understand the origin of dislocation structures in deformed crystals. Although the method was initiated over one decade ago, most of the original models were two-dimensional and consisted of periodic cells each

* Corresponding author. Tel.: +1-509 335 7832; fax: +1-509 335 4662.
E-mail address: zbib@mme.wsu.edu (H.M. Zbib)

0022-3115/00/$ - see front matter
PII: S0022-3115(99)00175-0

with dislocations of infinite length. These 2D models have provided some understanding of rules of interaction and glide mechanisms of dislocations. However, since these 2D models are based on the idealization of infinite dislocation lines, a number of important mechanisms and dislocation interactions are either not included in these models or accounted for in an implicit manner at best. These mechanisms include cross-slip, junction and jog formation, multiplication by Frank–Read sources, and line tension associated with self-energy. These difficulties have been addressed in a pioneering 3D dislocation model which was developed by Kubin and his co-workers [10] and Canova et al. [11]. Their model is based on the discretization of dislocation curves into a succession of pure edge and pure screw dislocation segments of fundamental length, corresponding to the discretized lattice. More recently, a new approach for 3D dislocation dynamics has been established by Zbib, Hirth and Rhee [12–14]. In this approach arbitrarily curved dislocations are decomposed into piecewise continuous arrays of mixed straight segments in a continuum crystal and long range interactions are treated using superdislocations, allowing for the treatment of large dislocation densities.

The 3D discrete dislocation model (mico3d) developed at WSU simulates the dynamical behavior of large numbers of dislocations of arbitrary shapes, interaction among groups of dislocations in 3D space and, therefore, the behavior of prescribed cell walls. In the model there is a number of rules and models for short-range reactions which, in turn, have a decisive effect on the predicted hardening and evolution of the structure. These issues have been, recently, addressed by Rhee et al. [13] who developed numerical rules for implementation into dislocation dynamics (DD) models to treat short-range interactions by introducing a critical force criterion. In this paper, we investigate these reactions and corresponding mechanisms that contribute critically to work hardening during deformation using the dislocation dynamics model. The main issues we address are junction formation and strength through the process of 'zipping' and 'unzipping', jog formation and strength, and dipole strength. It is shown that the full dynamics of these interactions can be explicitly captured via dislocation dynamics simulations, where the dynamics of these configurations is determined by direct calculation of driving forces and internal stresses. The simulation model is then utilized to provide possible explanations of irradiation induced hardening in metals subjected to cascade damage.

2. Basic equations

The complete description of the 3D dislocation model (DD) can be found in [12–14]. Here we give a brief outline of the main features of the model and basic governing equations. The main problem is that of nonlinear interaction of a large number of curved dislocations of arbitrary shapes. The crystal is treated as a continuum with dislocations restricted to move on crystallographic slip planes. The model has been developed for both fcc and bcc single crystals. For bcc single crystals we consider the $\{1\,1\,0\}\langle 1\,1\,1\rangle$ and $\{1\,1\,2\}\langle 1\,1\,1\rangle$ slip systems which are the most close packed slip systems and both kinds are active at low temperatures. The $\{1\,2\,3\}\langle 1\,1\,1\rangle$ slip systems are less close packed and become active at high temperatures. For fcc single crystals, $\{1\,1\,1\}\langle 0\,1\,1\rangle$ slip systems are considered, and hence glissile dislocation lines can only lie on the $\{1\,1\,1\}$ planes.

Each plane contains a number of dislocation curves and loops whose configurations are approximated by a series of straight segments of mixed character as illustrated in Fig. 1(a). There are a number of advantages in using mixed segments of arbitrary length and orientation:

1. Segment length depends upon the local curvature. Dislocation curves with small curvature are segmented with long segments, while those with large curvature are meshed with shorter segments (typical segment size could vary from $50b$ to a few hundred b, where b is the magnitude of the Burgers vector).

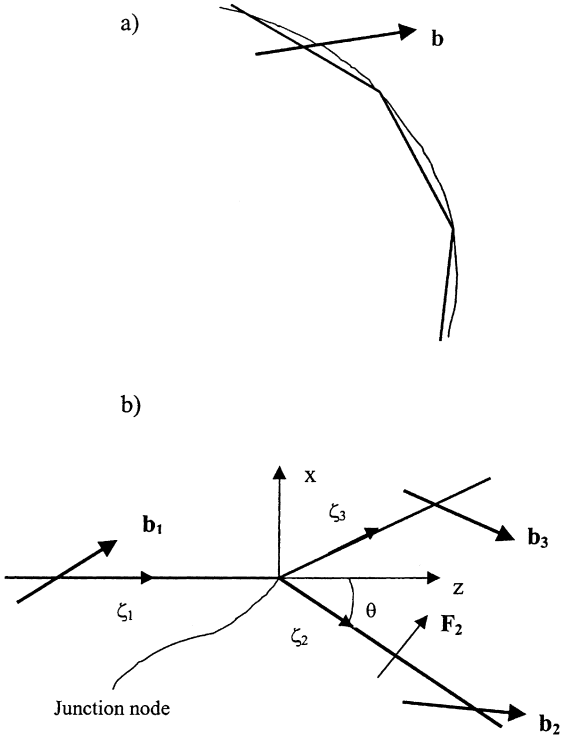

Fig. 1. (a) Discretization of a dislocation curve. (b) Dislocation bend or junction.

2. With mixed segments of arbitrary length and orientation, dislocation interactions such as junctions with any arbitrary configuration can be formed.
3. Mobility and strength of dislocation reactions, such as jog motion through dislocation bow-out at the jog and junction destruction by the process of 'unzipping' can be readily captured.
4. The stress field of arbitrary mixed straight dislocation segments in an isotropic medium is given in a closed form.

2.1. Long range interaction and self-force

The stress field of a finite dislocation segment is given by Hirth and Lothe [15] and deWit [16]. The interaction force per unit length (Peach–Koehler force 'PK force') a given segment exerts on a remote segment is evaluated at the center of the remote segment. This approximation is valid for two segments that are far apart from each other since the variation of the interaction force along the segment length is very small. For adjacent segments forming a bend the interaction force and self-force (or line tension) varies significantly along the dislocation line; it is singular at the bend and decays as $1/r$. Therefore, we treat this case in a more rigorous way as described by Zbib et al. [12]. The solution for the total interaction force between any two adjacent segments shown in Fig. 1(b) is developed following the same lines described by Hirth and Lothe [15] for a dislocation bend with the same Burgers vector. Here, the two segments could belong to the same dislocation line with the same Burgers vector, or they could have different Burgers vectors as in the case of dislocations meeting at a junction node. The result is an average glide force per unit length given by

$$\begin{aligned}\boldsymbol{F}_2 = \frac{\mu}{4\pi}\ln\left(\frac{L}{\rho}\right)\Bigg[&\boldsymbol{b}_{z1}\boldsymbol{b}_{z2}\frac{\cos\theta-1}{\sin\theta}-\boldsymbol{b}_{z2}^2\frac{v\sin\theta\cos\theta}{1-v}\\&+\boldsymbol{b}_{x1}\boldsymbol{b}_{z2}\frac{v}{1-v}+\boldsymbol{b}_{x2}\boldsymbol{b}_{z2}\frac{v}{1-v}\left(2\sin^2\theta-1\right)\\&+\boldsymbol{b}_{x1}\boldsymbol{b}_{x2}\frac{\cos\theta-1}{(1-v)\sin\theta}+\boldsymbol{b}_{x2}^2\frac{v\sin\theta\cos\theta}{1-v}\\&+\boldsymbol{b}_{y1}\boldsymbol{b}_{y2}\frac{\cos\theta-1}{(1-v)\sin\theta}\Bigg].\end{aligned}\tag{1}$$

The normal force component out of page is given by

$$\begin{aligned}\boldsymbol{F}_n = \frac{\mu}{4\pi(1-v)}\ln\left(\frac{L}{\rho}\right)\Bigg[&\boldsymbol{b}_{y1}\boldsymbol{b}_{x2}\frac{v\sin\theta+\cos\theta-1}{\sin\theta}\\&+\boldsymbol{b}_{x1}\boldsymbol{b}_{y2}\frac{\cos\theta-\cos^2\theta-v\sin^2\theta}{\sin\theta}\\&+\boldsymbol{b}_{z1}\boldsymbol{b}_{y2}(1-v)(1-\cos\theta)+\boldsymbol{b}_{y1}\boldsymbol{b}_{z2}v(2-\cos\theta)\\&-\boldsymbol{b}_{z2}\boldsymbol{b}_{y2}v\cos\theta+\boldsymbol{b}_{x2}\boldsymbol{b}_{y2}v\sin\theta\Bigg].\end{aligned}\tag{2}$$

Here μ is the elastic shear modulus, v the Poisson's ratio, L the dislocation segment length, and ρ the core parameter. For the case of general bend of two segments only (ignore segment '3' in Fig. 1(a)) $\boldsymbol{b}_1 = \boldsymbol{b}_2$ and Eqs. (1) and (2) reduce to the expressions given in [15]. In passing we emphasize that Eq. (1) accounts explicitly for the self-force which gives rise to the so called 'line tension'.

2.2. Dislocation mobility

The motion of each dislocation segment is determined by first evaluating the total PK force which arises from all other dislocation stress fields and the applied stress, such that

$$\boldsymbol{F}_i = \left(\sum_{\substack{j=1\\ j\neq 1\\ j\neq i+1\\ j\neq i-1}}^{N}\left(\sigma_j^{\mathrm{D}}+\sigma^{\mathrm{a}}\right)\cdot b_i\right)\times\xi_i + F_{i,i+1}+F_{i,i-1},\tag{3}$$

where N is the total number of dislocation segments, σ_j^{D} the stress tensor from a remote segment j, σ^{a} the applied stress tensor, ξ_i is the sense vector of segment i, and $F_{i,i+1}$ and $F_{i,i-1}$ the interaction forces between segments i and $i+1$, and i and $i-1$, respectively, as computed from Eqs. (1) and (2). The effective shear stress $\tau_{\mathrm{e}i}$ on segment i is given by

$$\tau_{\mathrm{e}i} = \frac{f_{gi}}{b}-\sigma_{\mathrm{f}},\tag{4}$$

where $f_{gi} = |\boldsymbol{F}_i\cdot\hat{\boldsymbol{v}}_i|$ is the magnitude of the glide force per unit length with $\hat{\boldsymbol{v}}_i$ being a unit vector in the direction of slip, and σ_{f} is the friction stress arising from lattice damping effects. The velocity vector of segment i is given by $\boldsymbol{v}_i = v_{gi}\hat{\boldsymbol{v}}_i$ where the basic relation for v_{gi} is discussed below.

The relationship between the glide velocity and the glide force per unit length (or effective shear stress) is temperature-dependent. At high temperatures, dislocations (pure edge, pure screw, and mixed ones) move by the phonon drag and climb mechanisms and the driving effective force is athermal. There are a number of relations for the dislocation glide velocity v_{g}, including relations of power law forms and forms with an activation term in an exponential or as the argument of a sinh form. Often, the simple power law form is adopted for expedience, e.g. $v_{\mathrm{g}} = v_{\mathrm{s}}(\tau_{\mathrm{e}}/\tau_{\mathrm{s}})^m$, where v_{s} and τ_{s} are constants. In a number of cases of pure phonon/electron damping control or of glide over the Peierls barrier a linear form of that equation, $m = 1$, predicts the results very well. The linear form has been theoretically predicted for a number of cases as reviewed by Hirth and Lothe [15] leading to

$$m^*\dot{v}_{gi} + v_{gi}/M_{gi} = F_g,$$
$$i = \text{e (for edge mixed dislocation)}$$
$$\text{or s (for screw dislocation)}, \tag{5}$$

where m^* is the effective mass and M_{gi} the dislocation mobility which, in general, depends on the character of the dislocation, especially at low temperatures. In bcc single crystals, at low temperatures a pure screw dislocation has a rather complex 3D core structure, resulting in a high Peierls barrier which may be overcome by stress-assisted thermal activation. This leads to a relatively low mobility for screw dislocations while the mobility of mixed dislocations is very high [17].

In a more general treatment, the inertia term should be included in Eq. (5). However, recent studies have shown that the rise time needed for a dislocation to reach a steady state is of the order of 10^{-10} s for a dislocation velocity below 0.4 times the shear-wave velocity [18]. A typical time step in computer simulation is of the same order, making it possible to neglect the inertia term, especially for low mobility dislocations in bcc metals. The inertia term, however, plays an important role for fast moving dislocations in fcc metals where the mobility is a few orders of magnitude higher than that in bcc.

The result of the above formulation is a set of nonlinear first-order differential equations governing the motion of the dislocation segments. The motion of the dislocations gives rise to plastic strain $\boldsymbol{D}^{\mathrm{p}}$ and spin $\boldsymbol{W}^{\mathrm{p}}$ which are calculated from

$$\boldsymbol{D}^{\mathrm{p}} = \frac{-1}{V}\sum_{i=1}^{N}[(\boldsymbol{v}_{gi}\times\xi_i)\otimes\boldsymbol{b}_i\ell_i]_{\mathrm{sym}},$$
$$\boldsymbol{W}^{\mathrm{p}} = \frac{-1}{V}\sum_{i=1}^{N}[(\boldsymbol{v}_{gi}\times\xi_i)\otimes\boldsymbol{b}_i\ell_i]_{\text{anti-sym}}, \tag{6}$$

where ℓ_i is the dislocation segment length, $\boldsymbol{v}_{gi}$ is the velocity of the segment, $\boldsymbol{b}_i$ the Burgers vector, ξ_i the line vector, and V is the volume of the simulated crystal.

2.3. Short range interactions

For short-range interactions, basic theories which describe the underlying physical mechanisms at the core level may be rigorously included into the 3DD model. Such an approach may be important when investigating the local interaction between two dislocations over small distances (close to the core). However, this approach is not desirable numerically or even important when dealing with relatively large numbers of dislocations on a large scale (10s of μm). Numerically, It is more efficient to develop rules based on a rigorous investigation of the two-dislocation interaction problem. Then, we implemented these rules directly into the 3DD model for large-scale simulations. These rules are:

Rule 1: Critical force criterion '$F \geqslant F^{\mathrm{c}}$' for short-range interaction.

Rule 2: Critical force criterion for annihilation.

Rule 3: Critical-angle criterion for junction formation; $\theta_{AB} \leqslant \theta^{\mathrm{c}}_{\mathrm{jn}}$.

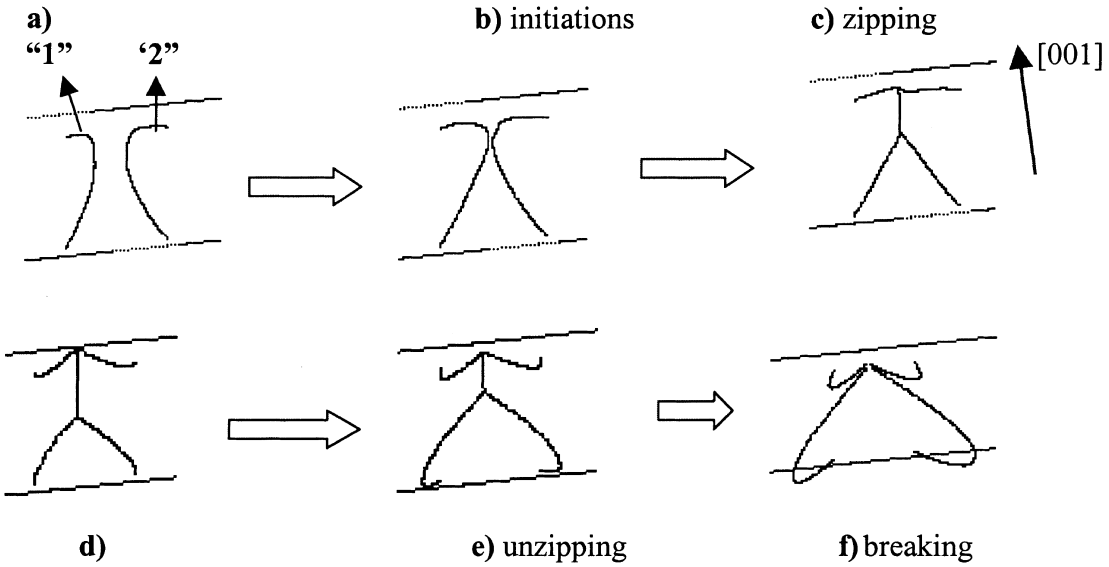

Fig. 2. (a)–(c) Junction formation 'zipping' with stress of 20 MPa applied in the [0 0 1] direction. (d)–(f) Junction destruction 'unzipping' with reversed stress (−30 MPa). Dislocation '1': $b/\sqrt{3}[\bar{1}\,1\,1](1\,1\,0)$; dislocation '2': $b/\sqrt{3}[1\,1\,\bar{1}](1\,\bar{1}\,0)$. Sessile junction is in the [0 0 1] direction with Burgers vector $2b/\sqrt{3}[0\,1\,0]$ ($2b/\sqrt{3}$ is the magnitude of the junction's Burgers vector).

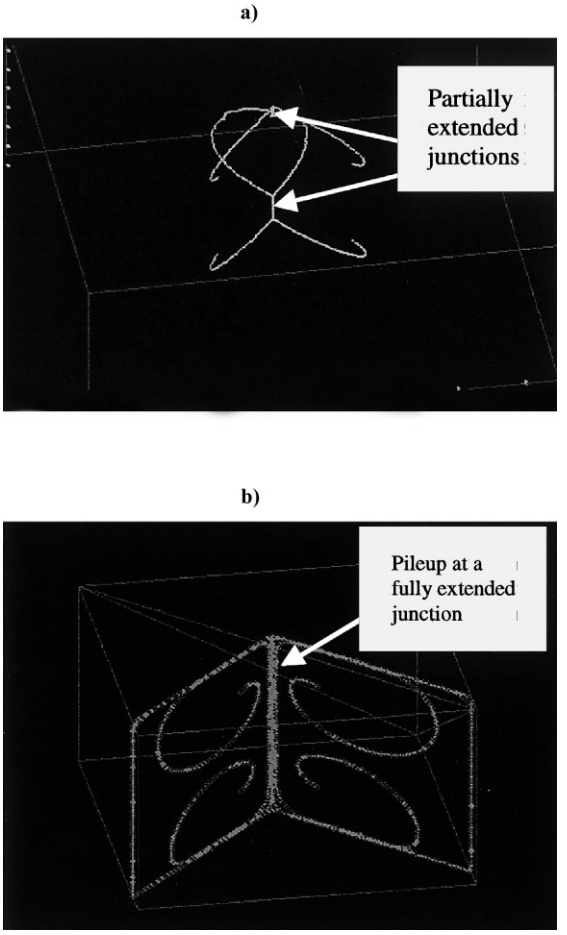

Fig. 3. (a) Formation of partial junctions and unzipping with stress increased (in the same sense) to 50 MPa. (b) A pileup of dislocations at a fully extended junction (the stress was not increased beyond 40 MPa).

Rule 4: Critical-angle criterion for jog formation; $\theta_{AB} \geqslant \theta^{c}_{jg}$.

Rule 5: Critical-angle criterion for jog strength; $\theta_{jg} \leqslant \theta^{c}_{jgs}$.

Here θ_{AB} is the angle between two dislocation segments, θ_{jg} the bow-out angle at a jog, and θ^{c}_{jn}, θ^{c}_{jg} and θ^{c}_{jgs} the *critical* values for junction formation, jog formation and jog strength, respectively. Each of these rules involves a critical value that determines the interaction. We suggest that numerical values for θ^{c}_{jn} and θ^{c}_{jg} should be determined from a rigorous investigation of the two-dislocation interaction problem, similar to that performed by Huang et al. [19] for the dipole problem. For now, however, we have estimated these values for a number of simplified case as reported in [13]. Values for the critical force, jog strength, as well as dislocation mobility maybe quantified explicitly by means of simulations at the core level, such as MD simulations [20]. These simulations could be very extensive since one would have to examine a number of possible combinations of the Burgers vectors and slip planes.

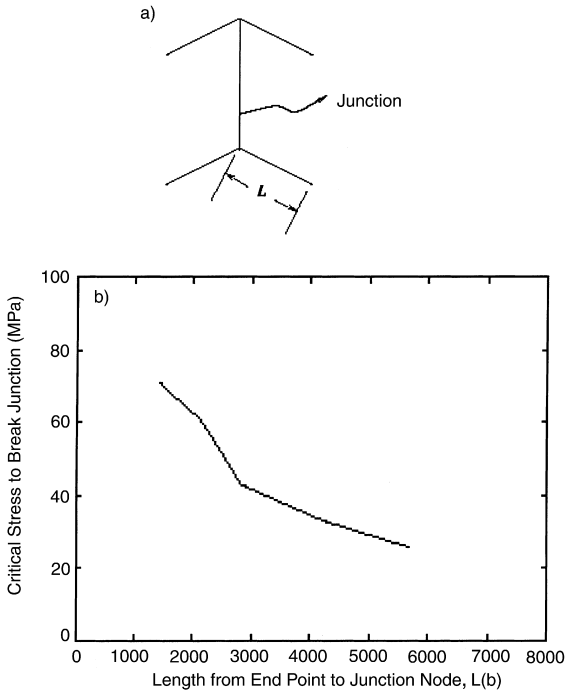

Fig. 4. (a) Fully extended junction formed as in Figs. 2(a)–(c), then the stress is reversed incrementally until the junction is completely destroyed as in Fig. 2(f). (b) The corresponding critical stress to break the junction as a function of L.

3. Basic reactions and strengthening mechanisms

In the following discussion we consider the deformation of a single crystal Ta (bcc crystallographic structure) at room temperature for which $b = 2.86 \times 10^{-10}$ m (here b is the magnitude of the $\langle 1\,1\,1 \rangle$ type Burgers vector), $\mu = 70.7$ GPa, $v = 0.339$, $\sigma_f = 3 \times 10^{-5}\mu$.

3.1. Junction formation – zipping

The process of dislocation junction formation has been addressed schematically by many authors, but no quantitative analysis has been performed except in the recent work of Bulatov et al. [21]. We studied this phenomenon using the DD dislocation dynamics model. The process begins when two attractive dislocations gliding on intersecting planes (Fig. 2(a)) meet at the line of intersection and combine if the reaction is favorable (Fig. 2(b)). In the DD simulations this is captured through explicit evaluation of the system dynamics,

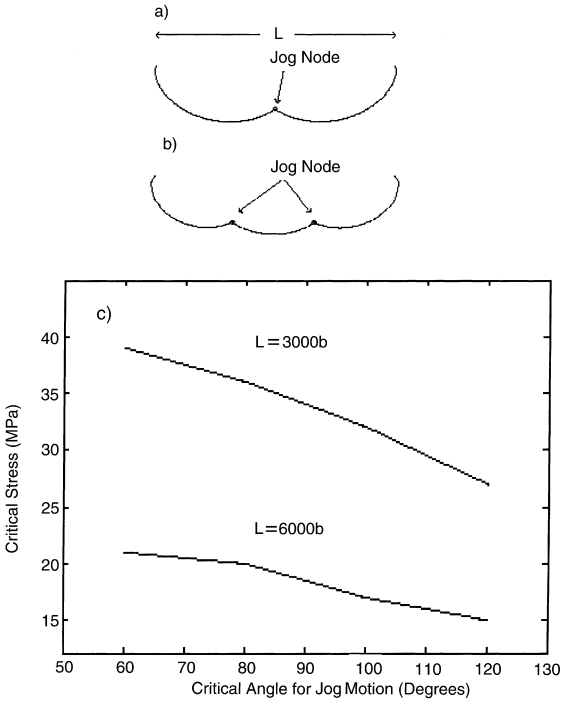

Fig. 5. (a), (b) Pinned dislocations with jogs. (c) Critical stress required to bow out and propagate the jogged dislocations as a function of jog critical angle (strength).

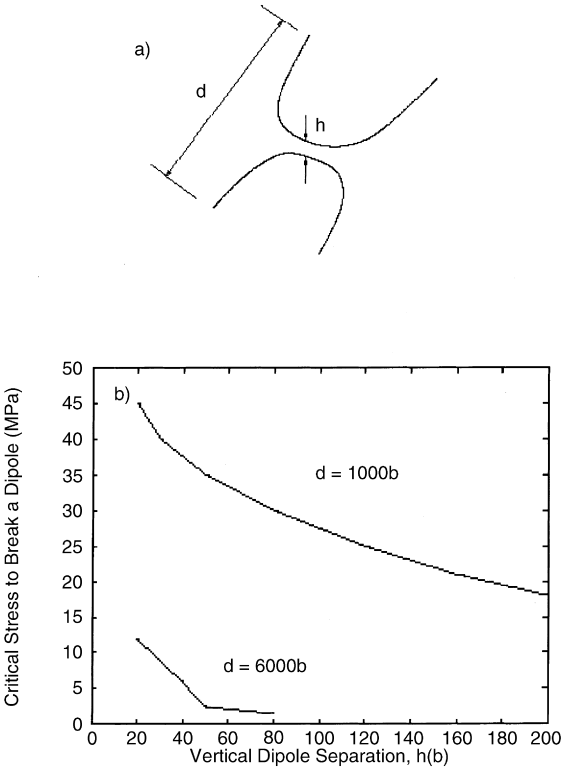

Fig. 6. (a) Two dislocations with opposite Burgers vectors emanating from two Frank–Read sources on parallel planes separated by distance h, forming a dipole 'lock' at distance $d/2$. (b) Critical stress to unzip the dipole.

i.e. there is no need to check if Frank's rule (i.e. $|b_1 + b_2|^2 < |b_1|^2 + |b_2|^2$) is satisfied before combining the segments. If the two segments are attractive (Rule 1) and their energy minimized by formation of a junction, they would approach each other, align themselves into a parallel configuration (Rule 3), react and form a junction. Once initiated, the junction extends along the line of intersection by the process of 'zipping' as anticipated by the Friedel–Saada model [22] (Fig. 2(c)). The configurations shown in Figs. 2(a)–(f) and 3(a), (b) are typical examples of junctions formed using DD simulations.

3.2. Junction destruction – 'unzipping'

The extension or destruction of the junction takes place by the motion of the dislocation node at the triple point along the line of intersection as anticipated by the Friedel–Saada model [22] and the recent MD simulations of Bulatov et al. [21]. This process is captured by DD simulations as shown in Figs. 2(d)–(f) and 3(a), (b). Thus, as also pointed out by Bulatov et al. [21], the force driving nodal stacking-fault energy determines the strength and fate of the junction.

The process of junction formation and destruction is a balance between applied stress, dislocation interaction forces and core energy around the junction node. As the reversed stress increases to a critical value the forces on the two dislocation nodes increase and move the nodes towards each other along the line of intersection. In the simulation, once the junction is formed and reaches a stable configuration as shown in Fig. 4(a), the applied stress is reversed incrementally. Due to the line tension effect, a higher stress is required to overcome the elastic interaction energy and core energy to unzip the junction. Fig. 4(b) shows the effect of line tension on the critical stress to unzip and break a junction. We can deduce from the figure that for a longer dislocation branch from the source (L) less force is required to overcome the elastic energy barrier for the unzipping process to occur. This is due to the fact that the force associated with line tension is larger with larger L, resulting in a higher self-force at the junction node.

3.3. Jog strength

Jogs can move by creating point defects such as vacancies or interstitials. The strength of these defects is balanced by the total line tension of the two dislocation

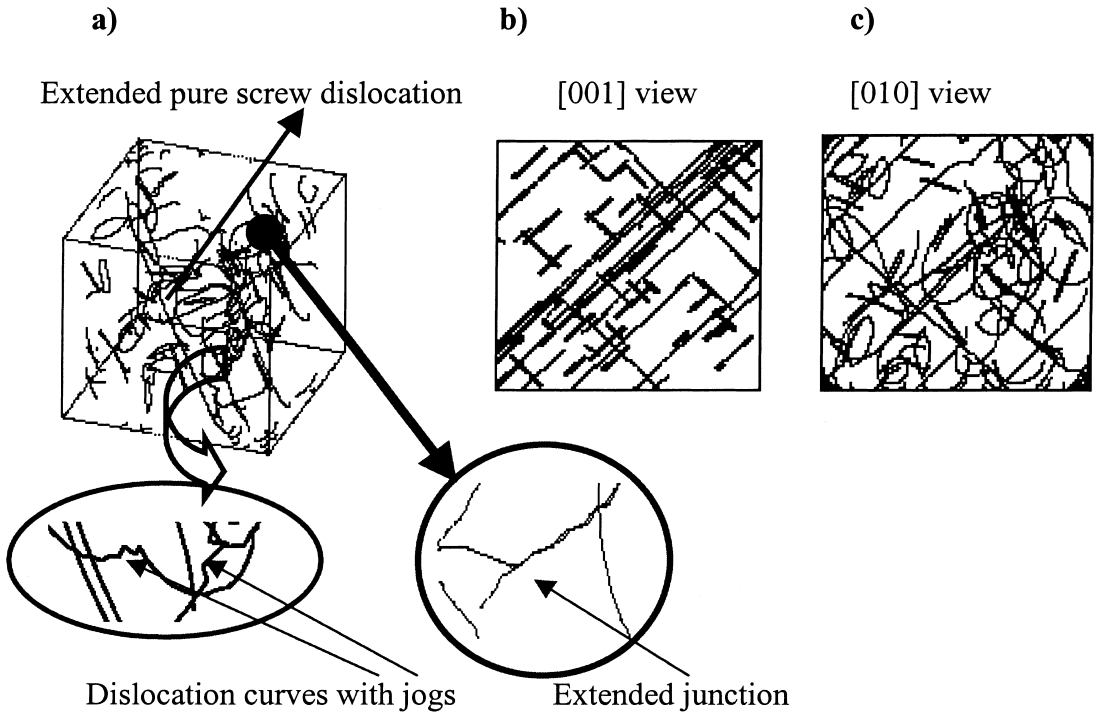

Fig. 7. (a) DD simulation of double slip deformation in Ta. (b) [0 0 1] view. (c) [0 1 0] view. Simulation cell side size = 10 μm.

segments surrounding a jog, leading to the following expression for the critical bow-out angle θ^{c}_{jgs} for a jog to move [15]

$$\cos\left(\frac{\theta^{c}_{jgs}}{2}\right) = \frac{W}{\mu b^3}, \tag{7}$$

where W is the interstitial or vacancy formation energy. To investigate the effect of the critical jog angle on the corresponding critical stress for jog motion, we carried out DD simulations for the configuration shown in Fig. 5. The result is obtained by considering a simple Frank–Read source with a jog located in the middle. For a given θ^{c}_{jgs} the stress is increased incrementally until the jog begins to move. Fig. 5(a) shows a snapshot of the simulation result after the jog has moved from its initial position. As the critical angle decreases, higher stress is required to move the jog as shown in Fig. 5(c). However, further decrease in the angle (less than 60°) does not result in a significant increase in the critical stress. This is because once the bow-out reaches the unstable configuration as in the Frank–Read source, less stress is required for the dislocation to wrap around the source. In the absence of a jog, the critical stress required to bow-out a Frank–Read source of length 6000b or 3000b is 11 MPa or 23 MPa, respectively. This value is, indeed, the minimum threshold for the critical stress to bow-out the Frank–Read source with a very weak jog, corresponding to a critical jog angle approaching 180°.

3.4. Dipole strength

Although models describing the dipole strength are available, the dipole is usually assumed to be infinitely long. In our approach, dipole break occurs naturally if the stress required to cause it is sufficient. Consider, for example, the dipole which is formed by the bow-out of dislocations from Frank–Read, as sources shown in Fig. 6(a). The strength of the dipole depends on the normal separation h and the separation d between original sources.

Fig. 6(b) shows the critical stress to unzip a dipole as a function of the normal separation and the separation between the original sources. For a constant dipole separation h, a dipole with a smaller d value requires higher stress to break. This is due to the line tension from the dipole to the pinning point. For larger d the curvature of the dislocation at the dipole position is larger. This, in turn, results in a larger line tension, making it easier to unzip the dipole, similar to the case of junction unzipping. Furthermore, we note that, due to the line tension, the critical shear stress to

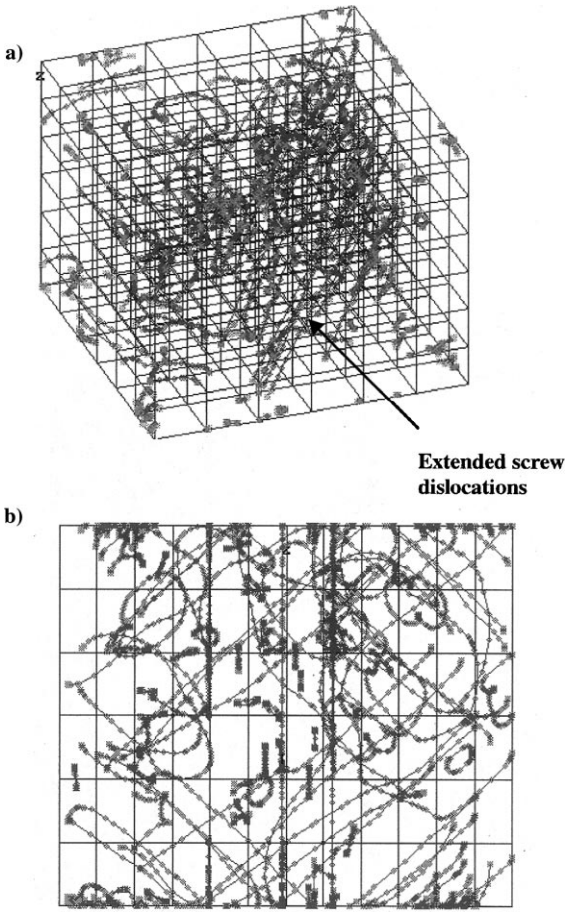

Fig. 8. (a) DD simulation of double slip deformation in Mo. (b) [1 1 0] view. Simulation cell size = 30 μm.

break the dipole is much smaller than that predicted for the case of two infinite dislocation segments, which is given by

$$\tau_c = \frac{\mu b}{8\pi(1-\nu)}\frac{1}{d}. \tag{8}$$

4. Double slip deformation

In this section we present typical results of the deformation of single crystals. Fig. 7(a) shows a cubic cell of side size 10 m. In this case, the simulated material is a Ta single crystal whose properties are given in Section 3. The crystal contains 50 Frank–Read sources distributed randomly on the two slip planes (1 1 0) and $(\bar{1}\,1\,0)$, as shown in Fig. 7. For each plane, there are two possible Burgers vectors of the type $\langle 1\,1\,1\rangle$ and, therefore, the Burgers vector for each dislocation is assigned randomly. The size of the dislocation sources (i.e. the distance between the two pinning points in the Frank–Read source) varies from $5000b$ to $8000b$. This gives an initial dislocation density of 10^{11} m^{-2}. The load is applied along the [1 0 0] direction with a constant strain rate of 10 s^{-1}. The resolved shear stresses on both planes are equal, activating both slip systems. The mobility of edge and mixed dislocations is 10^2 (Pa s)$^{-1}$ and that of screw ones is assumed to be smaller by one order of magnitude. A snapshot of the dislocation substructure after 163 000 iterations is shown in Fig. 7. As a result of dislocation intersections, many jogs and junctions form and their total number increases with further deformation (the total number of jogs in Fig. 7 is 184). The simulation is performed for a jog critical angle (strength) of 120°. The dislocation density in Fig. 7 is 4.3×10^{11} m^{-2}. In passing we point out that using low strain rates, say in the order of 10^{-4} s^{-1}, would be more consistent with typical experiments but this introduces severe numerical limitations on the DD simulations due to required integration time steps. However, this numerical issue is currently being addressed.

Fig. 8 shows results obtained for a molybdenum single crystal (bcc) deformed at room temperature with loading applied along the [0 0 1] direction. The simulation was performed for two cell side sizes, 30 μm and 10 μm. For Mo: $b = 2.725\times10^{-10}$ m (for the $\langle 1\,1\,1\rangle$ Burgers vectors) $\mu = 123$ GPa, $\nu = 0.305$, $\sigma_f = 3\times10^{-5}\mu$. The mobility of edge and mixed dislocations is 10^3 (Pa s)$^{-1}$ and that of screw ones is assumed to be 2.5 (Pa s)$^{-1}$. This estimate is based on the experimental results of Prekel and Conrad [23]. The low mobility of the screw segment results in a dislocation substructure dominated by extended screw dislocations as can be deduced from Fig. 8. This result is consistent with typical TEM observations [23]. The corresponding stress strain curve obtained from the DD simulations is given in Fig. 9(a). We note that the serrations in the curve have no physical meaning. They result from a number of factors including, cell size, strain rate, and a balance between the rate of annihilation of dislocations at the boundary of the cell and dislocation production from Frank–Read sources. In this respect, we point out that these serrations can be smeared out by increasing the size of the cell and increasing the initial dislocation density. Nevertheless, we can extract from this figure a value for the initial yield stress (for strain rate of 10 s^{-1}) of 70 MPa. Moreover, we also obtain an average strain hardening of 2500 MPa (slope of the line shown in the figure). This strain hardening can be attributed mainly to an increase in the number of jogs and in the dislocation density during deformation. The change in the dislocation density and number of jogs is given in Figs. 9(b) and (c), respectively. The dislocation density increases towards a saturation value as the strain increases.

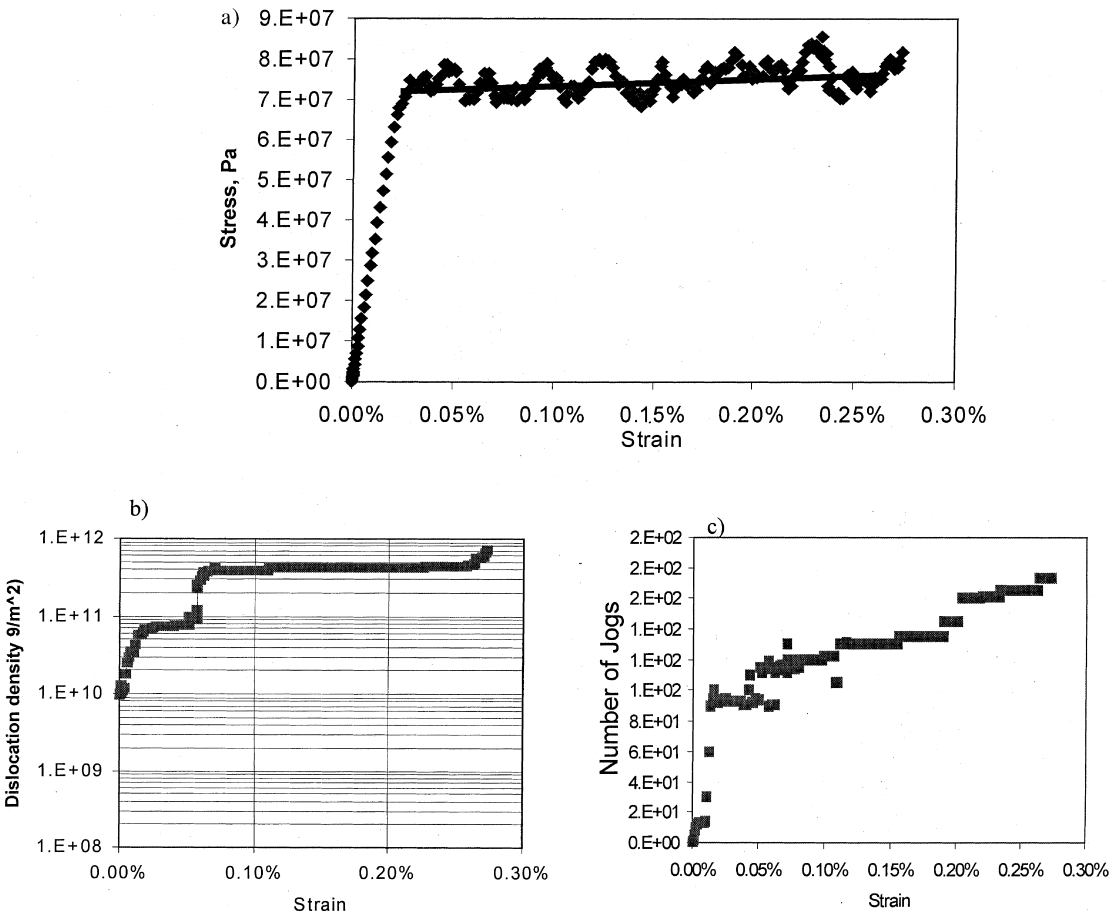

Fig. 9. DD results for double-slip deformation of a single crystal Mo with cell side size = 10 μm, Strain rate = 10 s^{-1}. (a) Stress–strain curve. (b) Dislocation density. (c) Number of jogs.

5. Irradiation induced hardening

Finally, we consider the problem of irradiation induced hardening problem in single crystals subjected to cascade damage. In order to illustrate the possibility of the DD simulation in providing rigorous explanation of this phenomenon, we consider here the defect structure in irradiated Cu. The substructure after irradiation consists of prismatic dislocation loops resulting from collapse of vacancies or interstitials [24–29] (stacking-fault tetrahedrons are not considered here but will be included in future investigations). The main issue we look into is the phenomenon of increased yield stress resulting from irradiation. The subsequent phenomena of yield drop and localized deformation will be investigated later.

As pointed out by Trinkaus et al. [28], the irradiated induced hardening cannot be rationalized in terms of conventional dispersion hardening. However, this phenomenon may be understood in terms of cascade induced source hardening in which the dislocations are considered to be locked by the loops decorating them. Fig. 10(a) shows a dislocation decorated by loops as described in [28]. For an infinite dislocation, the critical stress to unlock the dislocation is approximated by [28] as

$$\sigma_y \cong 0.069 \frac{\mu}{1-\nu} \frac{b}{L} \left(\frac{d}{y} \right)^2. \tag{9}$$

For definition of L, d, y see Fig. 10(b). For Cu with $\mu = 55$ GPa, $\nu = 1/3$, $L = 200b$, $d/y = 3/2$, and Eq. (9) yields $\sigma_y = 61$ MPa. However, when we consider a finite dislocation pinned at both ends as in a Frank–Read Source, the critical stress required to unlock the dislocation depends upon the dislocation length as well as the loop structure. This was shown using the DD simulation (see Figs. 10(c) and (d)). In Fig. 10(c) the dislocation becomes unstable when the stress reaches 100 MPa. In this case the dislocation is not decorated with loops.

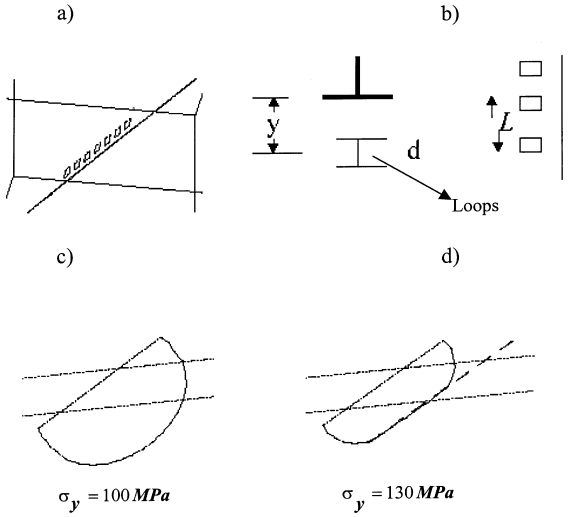

Fig. 10. (a) Prismatic dislocation loops decorating a dislocation in Cu. (b) Side view (y = stand-off distance, $d = 30b$ is the loop size, $L = 200b$). (c) Dislocation propagating from a Frank–Read source, which is not pinned by dislocation loops. (d) Dislocation propagating from a Frank–Read source, which is pinned by dislocation loops.

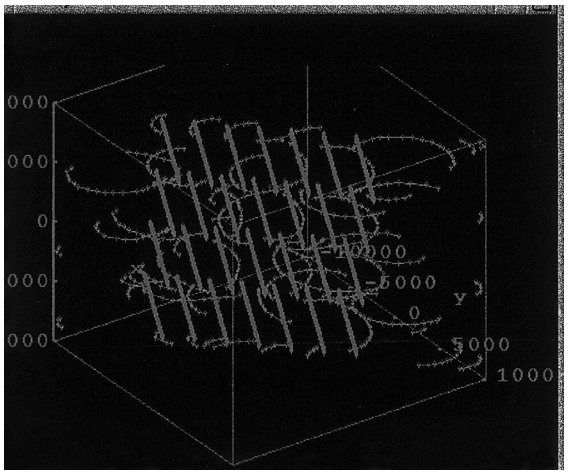

Fig. 11. Simulation of dislocations decorated with dislocation loops in Cu. Cell side size = 10 μm, loop density = 10^{19} m^{-3}.

However, when the dislocation is decorated with loops the yield stress increases to 130 MPa, which is larger than the value predicted by the simple model given by Eq. (9), i.e. 61 MPa. This significant difference can be attributed to the line tension effect associated with the dislocation bow-out which is captured by the DD simulations but not by the simple model.

The results just presented illustrate the basic mechanism of hardening as captured by the DD simulation. Full analyses with large dislocation densities and various distributions are currently under way. Two possible models are being analyzed: (1) sessile dislocation loops decorating the dislocations model (strong obstacles), and (2) the dispersions hardening model with sessile dislocation loops (weak obstacles) distributed randomly in the material. Preliminary results are shown in Figs. 11 and 12. In Fig. 11 we show a periodic distribution of sessile loops decorating dislocations with a loop density of 10^{19} m^{-3}. For random distribution of loops (dispersion hardening model), the dislocation percolates around the obstacles (sessile loops) as shown by the DD simulation and given in Fig. 12. Typical predicted stress–strain curves using the decorated dislocations model are shown in Fig. 13, revealing the effect of dislocation loops in increasing the yield stress. It is emphasized that these are very preliminary results and detailed analysis needs to be performed before drawing any significant conclusions. Our attempt here is to develop a unified model combining the two mechanisms (loops decorating the dislocations and random distribution of loops) which would be more consisted with experimental observations. However, these preliminary results illustrate the potential of the DD simulations in providing answers to a number of critical questions related to irradiation induced hardening and associated phenomena. This includes, the correct scaling between the yield stress and defect density, yield drop and localized deformation, etc. Detailed analyses along these lines are now underway.

6. Conclusions

Basic dislocation mechanisms that contribute to yielding and strain hardening in metals have been investigated using dislocation dynamics. These mechanisms include dipole formation, dislocation intersections (junctions and jogs formation), and dislocation–irradiation-induced-defect interactions (cascade damage). These mechanisms were studied according to DD rules and models that have been developed to treat short-range reactions in bcc and fcc metals. The results suggest that the DD simulation model provide a very valuable tool for investigating critical dislocation phenomena that control plastic deformation and hardening in metals. This type of microscopic modeling of deformation provides a natural transition from the atomic scale to the continuum crystal scale. It is suggested that, while MD simulations may provide needed rules for dislocation dynamics and interactions based on fundamental principles, DD simulations can provide the most rigorous means for understanding the impact of these critical mechanisms from the dislocation length scale to the macroscopic scale.

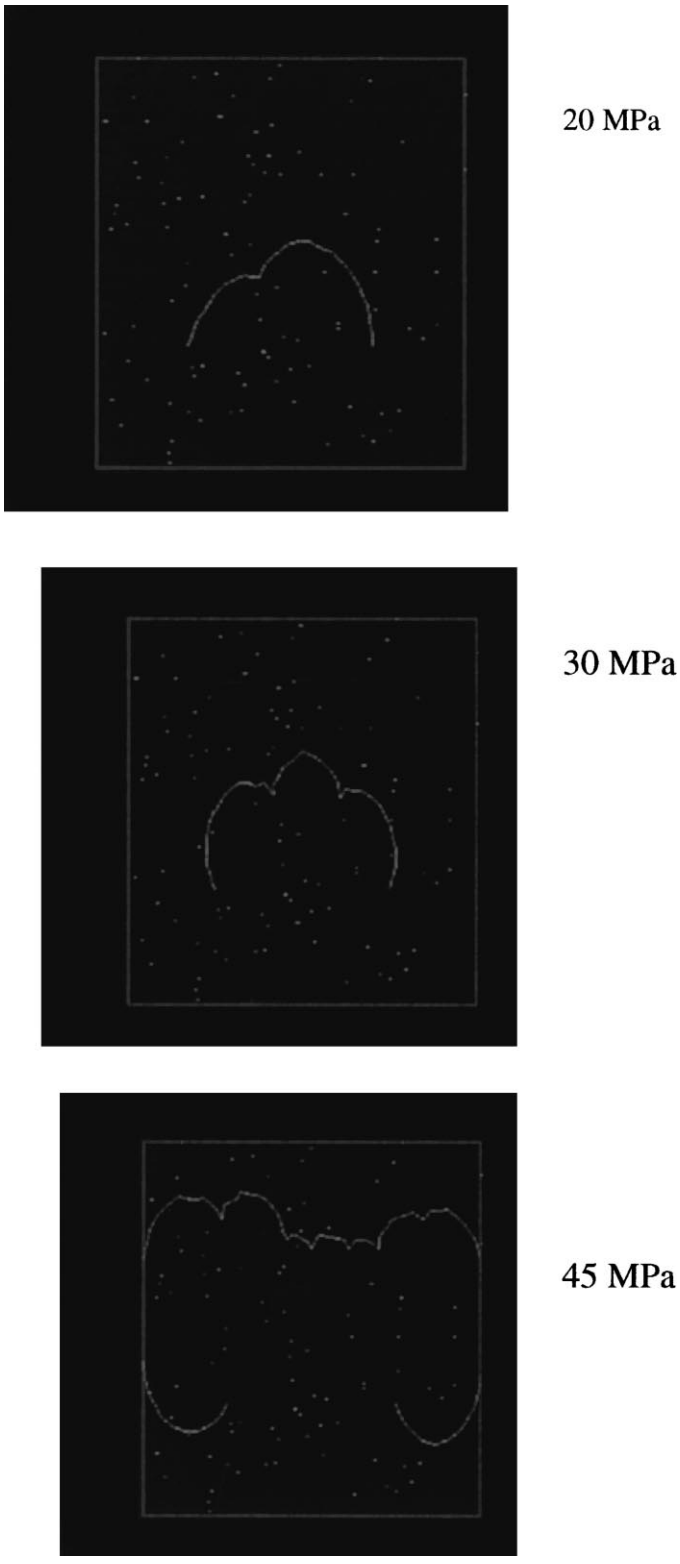

Fig. 12. Dislocation percolation around loops (dispersion harening model). The stand-off distance between the plane of the dislocation and the plane of the loops is 5*b*.

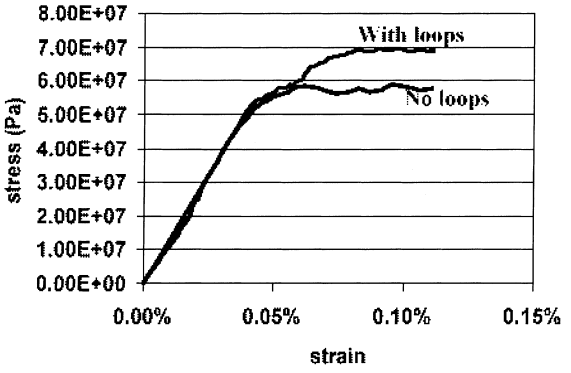

Fig. 13. Predicted stress–strain curves for the case of loops decorating the dislocations, showing the effect of dislocation loops in an irradiated material (Cu) on yield stress.

Acknowledgements

The support of the Lawrence Livermore National Laboratory under contract No. W-7405-ENG-48 with the DOE, is gratefully acknowledged.

References

[1] S. Mader, A. Seeger, H.M. Thieringer, J. Appl. Phys. 34 (1963) 3376.
[2] H. Mughrabi, Mater. Sci. Eng. 85 (1987) 15.
[3] M.S. Whelan, in: P.B. Hirsch, (Ed.), The Physics of Metals, Part 2: Defects, Cambridge University, London, 1975, p. 98.
[4] U. Essmann, H. Mughrabi, Philos. Mag. A 40 (6) (1979) 731.
[5] P.J. Woods, Philos. Mag. 28 (1973) 155.
[6] N. Hansen, D. Kuhlmann-Wilsdorf, Mater. Sci. Eng. 81 (1986) 141.
[7] D. Kuhlmann-Wilsdorf, Mater. Res. Innovat. 1 (1989) 265.
[8] D. Holt, J. Appl. Phys. 41 (1970) 3197.
[9] E.C. Aifantis, Sol. Stat. Phenom. 3&4 (1988) 397.
[10] L.P. Kubin, Phys. Stat. Sol. (A) 135 (1993) 433.
[11] G.R. Canova, Y. Brechet, L.P. Kubin, in: S.I. Anderson et al (Eds.), Modelling of Plastic Deformation and Its Engineering Applications, Risø National Laboratory, Roskilde, Denmark, 1992.
[12] H.M. Zbib, M. Rhee, J.P. Hirth, Int. J. Mech. Sci. 40 (1998) 113.
[13] M. Rhee, H.M. Zbib, J.P. Hirth, Modeling Simul. Mater. Sci. Eng. 6 (1998) 467.
[14] J.P. Hirth, M. Rhee, H.M. Zbib, J. Computer-Aided Mater. Des. 3 (1996) 164.
[15] J.P. Hirth, J. Lothe, Theory of Dislocations, Wiley, New York, 1982.
[16] R. de Wit, Phys. Stat. Sol. 20 (1967) 567.
[17] N. Urabe, J. Weertman, Mater. Sci. Eng. 18 (1975) 41.
[18] J.P. Hirth, H.M. Zbib, J. Lothe, Modeling Simul. Mater. Sci. Eng. 6 (1998) 165.
[19] H. Huang, N. Ghoniem, T. Diaz de la Rubia, M. Rhee, H.M. Zbib, J.P. Hirth, ASME-JEMT 121 (1998) 143.
[20] S.J. Zhou, D.L. Preston, P.S. Lomdahl, D.M. Beazley, Science 279 (1998) 1525.
[21] V. Bulatov, F.F. Abraham, L. Kubin, B. Devincre, S. Yip, Nature 392 (1998) 669.
[22] J. Friedel, Dislocations, Pergamon, Oxford, 1964.
[23] H.L. Prekel, H. Conrad, in: Rosenfield et. al. (Eds.), Dislocation Dynamics, McGraw-Hill, New York, 1968.
[24] R.L. Fleischer, Acta Metall. 10 (1962) 835.
[25] P.B. Hirsch, in: R.E. Smallman, J.E. Harris (Eds.), Vacancies 76, The Metals Society, 1976, p. 95.
[26] J. Friedel, Dislocations, Oxford Press, Oxford, 1964, p. 225.
[27] U.F. Kocks, Philos. Mag. 13 (1966) 541.
[28] H. Trinkaus, B.N. Singh, A.J.E. Foreman, J. Nucl. Mater. 251 (1997) 172.
[29] Y. Dai, thesis No. 1388, Ecole Ploytechnique Federale de Lausanne, 1995.